Noncontact backscatter-mode near-infrared time-resolved imaging system: preliminary study for functional brain mapping

Ichiro Sase
Akira Takatsuki
National Institute of Information and Communications Technology
Kansai Advanced Research Center
Brain Information Group
588-2 Iwaoka, Nishi-ku, Kobe
Hyogo 651-2492, Japan

Junji Seki
National Cardiovascular Center Research Institute
Department of Biomedical Engineering
5-7-1 Fujishiro-dai, Suita
Osaka 565-8565, Japan

Toshio Yanagida
Akitoshi Seiyama
National Institute of Information and Communications Technology
Kansai Advanced Research Center
Brain Information Group
588-2 Iwaoka, Nishi-ku, Kobe
Hyogo 651-2492, Japan
and
Osaka University
Graduate School of Medicine
Division of Physiology and Biosignaling
2-2 Yamadaoka, Suita
Osaka 565-0871, Japan

Abstract. To improve the spatial resolution and to obtain the depth information of absorbers buried in highly scattering material, we developed a noncontact backscatter-mode near-infrared time-resolved imaging system (noncontact B-TRIS) that is intended for functional human brain mapping. It consists of mode-locked Ti-sapphire lasers as light sources and a charge-coupled device camera equipped with a time-resolved intensifier as a detector. The system was tested with a white polyacetal phantom as a light-scattering medium and black polyacetal particles as absorbers. Illumination and detection of light through an objective lens system (ϕ=150 mm) enabled us to capture images from an area whose diameter is about 70 mm without coming into contact with it. The scattering and absorption coefficients of the white phantom obtained by B-TRIS were similar to those obtained by a conventional time-resolved spectroscopy. Although the imaged diameter of an absorber buried within a phantom was considerably larger than the actual diameter, the center position of the absorber coincided with the actual position with accuracy $<$2 mm. Furthermore, the depth information can be also detected by the noncontact B-TRIS. These results suggest a potential of noncontact B-TRIS for imaging cognitive human brain function. [DOI: 10.1117/1.2363359]

Keywords: biomedical optics; imaging; laser applications; infrared imaging; optical systems; optical testing.

Paper 05173RRR received Jul. 2, 2005; revised manuscript received May 26, 2006; accepted for publication May 31, 2006; published online Oct. 20, 2006.

1 Introduction

Simultaneous measurements of a near-infrared imaging technique with other noninvasive functional neuroimaging techniques revealed that near-infrared optical measurement has become one of the important tools for understanding human brain activities.[1–3] One significant feature of the optical method is that near-infrared spectroscopy (NIRS) can provide the redox state of the terminal mitochondrial enzyme cytochrome *c* oxidase noninvasively as well as changes in concentrations of deoxygenated and oxygenated hemoglobin, which occurs in the human cerebral cortex in response to neural activity.[4] Another important feature is that the optical system does not restrict subjects in a constrictive imaging chamber during measurements, so the system could be applied to measurements of brain activations induced by various types of tasks, such as gait tasks,[5] visual stimulation of infants,[6] and metal tasks with a written test,[7] as well as those of higher-order brain functions.[8–10] Furthermore, the optical method is now applied to detect the fast responses linked with electrophysiological phenomena,[11–13] which more directly reflects the neuronal activity in the human cerebral cortex.

Most conventional NIRS imaging systems utilize several pairs of optical fibers for the irradiation and detection of light to provide surface-projection images of an object. However, those multiple fiber systems have the following disadvantages:[14,15] (1) spatial resolution and sensitivity depend on the location of the optical fibers, and (2) the signal-to-noise (S/N) ratio is affected by the attachment or angle of the fiber tip against the skin (or the subject). As NIRS is increasingly applied to clinical and cognitive neuroscience, these issues have come to be pointed out more often. Furthermore, it is important to improve spatiotemporal resolution of NIRS to obtain more "precise functional mapping" of the brain by expanding the use of the features of light, such as wavelength, polarization, intensity, and traveling time. Thereby, we expect a new insight into unexplained brain functions such as the "sensory motor paradox" during tactile stimulation,[16] pain examinations,[17] and imagery experiments,[18] which are occasionally difficult to detect by conventional brain mapping techniques such as functional

Address all correspondence to Akitoshi Seiyama, Osaka University, Graduate School of Medicine, Division of Physiology and Biosignaling, 2-2 Yamadaoka, Suita, Osaka 565-0871, Japan. Tel: +81-6-6879-4632; Fax: +81-6-6879-4634; E-mail: aseiyama@phys1.med.osaka-u.ac.jp

1083-3668/2006/11(5)/054006/7/$22.00 © 2006 SPIE

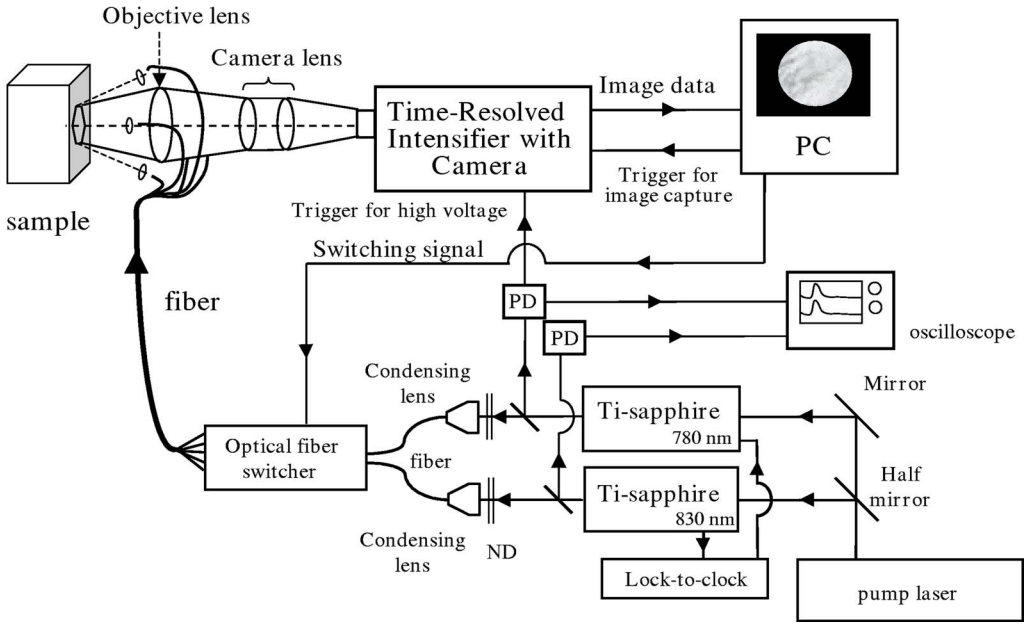

Fig. 1 Block diagram of noncontact B-TRIS system.

magnetic resonance imaging (fMRI) and position emission tomography.

Recently, various attempts have been made to improve spatial resolution and/or quantification of NIRS signals using fiber optical systems[19–21] and noncontact systems[22–26] based on continuous wave[19,23,24] and time[20,21,25] or frequency[22,26] domain methods.

Advantages of the time-resolved optical measurement system have been demonstrated by many fundamental experiments trying to evaluate the contrast-to-noise ratio (i.e., sensitivity) by varying inclusion depth[20] or source to detector distance[21] and the resolving power of optical tomographic schemes using fast-transmitted photons of ultrashort pulses[27] and by trying to calculate path length for adopting the modified Lambert-Beer equation using the time-of-flight value.[28]

In the present study, we have developed a noncontact type of backscatter-mode time-resolved imaging system (noncontact B-TRIS) to overcome the problems mentioned before. We have assembled a reflective imaging system and demonstrated its merits when detecting and mapping light-absorbing particles buried inside the scattering media. There are several merits of noncontact B-TRIS:

(1) Direct visualization of absorbers at their actual positions, without any complicated calculations or interpolations.

(2) Improvement of spatial resolution resulting from liberation from the restriction of fiber positioning.

(3) Noncontact detection (without attachment of optical fibers to the skin).

(4) Detection of depth information by time window (detection of Z position and improvement of S/N ratio by volume limitation).

We tested the above four items with noncontact B-TRIS using a polyacetal phantom. In this paper, we discuss the development of this technology to apply it to human brain mapping in comparison with the conventional multichannel NIRS.

2 Materials and Methods

2.1 *Camera System*

A schematic drawing of a reflective-mode time-resolved optical imaging system is shown in Fig. 1. Two sets of mode-locked Ti-sapphire lasers (Tsunami, Spectra-Physics Lasers, USA), which are tunable to conventionally used wavelengths to measure brain activity (e.g., 780, 805, or 830 nm; 80 MHz, 10 to 16 ps, 800 to 1100 mW), were used as light sources. Pulsing of the 730-nm laser was synchronized with that of the 830-nm laser by a lock-to-clock system (Lock-to-clock, Spectra-Physics Lasers). Stabilities of laser pulsing were monitored by a photodiode (PD). Both lasers are guided into separate optical fiber switchers (F-SM19, Piezosystem Jena GmbH, Germany) through objective lenses. One laser pulse within 1 sec was incident on one optical fiber, and it was switched to the other optical fibers one by one by an optical fiber switcher controlled by a personal computer (PC). Each optical fiber output was introduced into a set of optical elements that consisted of a ball lens, iris, and convex lens, which collimate output beams [Fig. 2(b)]. Laser powers were reduced to 1/100 by neutral density (ND) filters placed immediately after the laser output. Then, the laser beams were led to the optical switching system. Each laser power at the sample surface was also adjusted to 100 μW by the output iris. Pulse width at the sample was around 100 ps (initial laser pulse widths were about 10 to 15 ps).

Images were captured by a charge-coupled device (CCD) camera (Imager3, LaVision GmbH, Germany) equipped with a time-resolved intensifier (Picostar, La Vision). Laser output triggered a high-voltage gate pulse for the time-resolved intensifier. Timing of image acquisition and laser illumination was controlled by the PC. Acquired images were transferred to the PC independently from laser pulse timing (80 MHz $\gg$ 10 to 100 Hz) and analyzed by a separate soft-

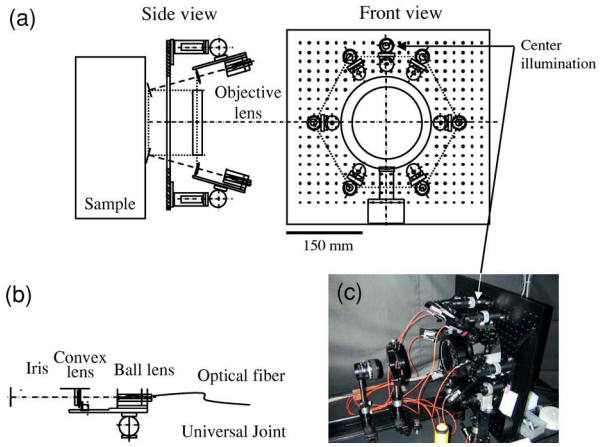

Fig. 2 Noncontact illumination system. (a) Schematic drawing of the optical system around the sample. (b) Laser illumination assembly. (c) Photographic image of entire optical assembly.

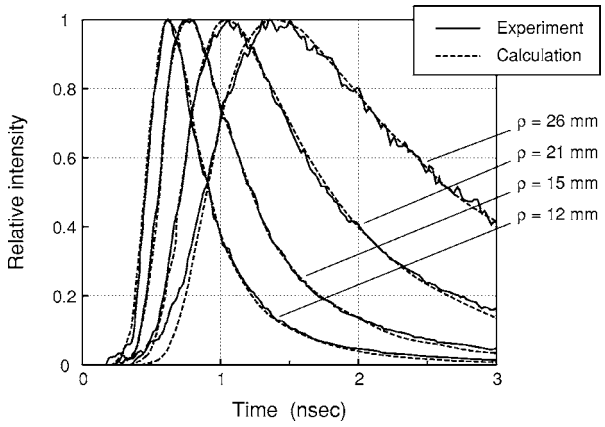

Fig. 3 Temporal profiles of light intensity at 780 nm reflected by large bulk phantom (solid lines) and fitting curves (dashed lines) using Patterson's half infinite model (Ref. 29) assuming refractive index (n) of the phantom was 1.48. Measurements were performed every 25 ps. Light intensities, detected at distance (ρ) of 12, 15, 21, and 26 mm from light illumination spot, were integrated over 3×3 mm^2 of the detection area. Estimated optical properties of the phantom are shown in Table 1.

ware (Image Pro Plus, Media Cybernetics, USA).

2.2 *Noncontact Illumination System*

To achieve noncontact illumination, we have prepared a light illumination assembly [Figs. 2(a)–2(c)] encircling an objective lens [f=150 mm, diameter (ϕ)=150 mm, borosilicate crown glass (BK7), antireflection (AR) coated]. A schematic drawing of the optical system around the sample is shown in Fig. 2(a). The sample in the drawing is a large phantom block and the signal from the phantom is imaged by the objective lens through a large aperture on the upright optical bench. The sample image is relayed by a combination of the objective lens, and two sets of camera lenses (Nikkor 50 mm F1.2S, Nikon, Japan). The upright optical bench board holds multiple laser illuminating assemblies shown in Fig. 2(b). The laser beam emanating from the optical fiber is collimated by the ball lens and focused on the sample surface by a convex lens and iris to a spot with a diameter less than 1 mm. Time lags of the laser output between each optical fiber caused by the optical switcher were between 25 and 200 ps. However, fibers with the closest output times were selected so that the time difference was maintained at less than 50 ps for every experiment. A photograph of the optical assembly is shown in Fig. 2(c). Orange fibers are the incident optical fibers from a fiber switcher. In the present study, the distance between the phantom surface and the detector (and the convex lens for illumination) depends on the focal length of the objective lens (f =150 mm), and the distance between the phantom surface and CCD was about 700 mm.

3 Results

In the present study, we evaluated a noncontact B-TRIS to measure optical properties of scattering media and resolving

Table 1 Optical properties obtained with near-infrared time-resolved spectroscopy.

	B-TRIS		TRS-10	
Distance between Input and Output	$\mu s'$[a] (mm^{-1})	μa[b] ($\times 10^{-3}$ mm^{-1})	$\mu s'$[a] (mm^{-1})	μa[b] ($\times 10^{-3}$ mm^{-1})
15 mm	1.01	1.36	nd[c]	nd
21 mm	1.10	0.98	nd	nd
26 mm	0.96	0.95	nd	nd
30 mm	nd	nd	1.00	0.59
40 mm	nd	nd	0.97	0.61

[a] $\mu s'$, scattering coefficient.
[b] μa, absorption coefficient. Optical properties of a bulk white polyacetal were measured with a noncontact B-TRIS instrument and conventional time-resolved spectroscopy [TRS-10, Hamamatsu Photonics, Japan (Ref. 30)]. The values for noncontact B-TRIS show the results obtained at 780 nm, and the values for TRS-10 show the mean value of the results obtained at 761 and 795 nm.
[c] nd: not determined (data for distances longer than 30 mm could not be obtained by B-TRIS due to low signal intensity and low S/N ratio, and the data for distances shorter than 26 mm could not be obtained by TRS-10 due to strong reflected light intensity greater than the sensitivity of the detector).

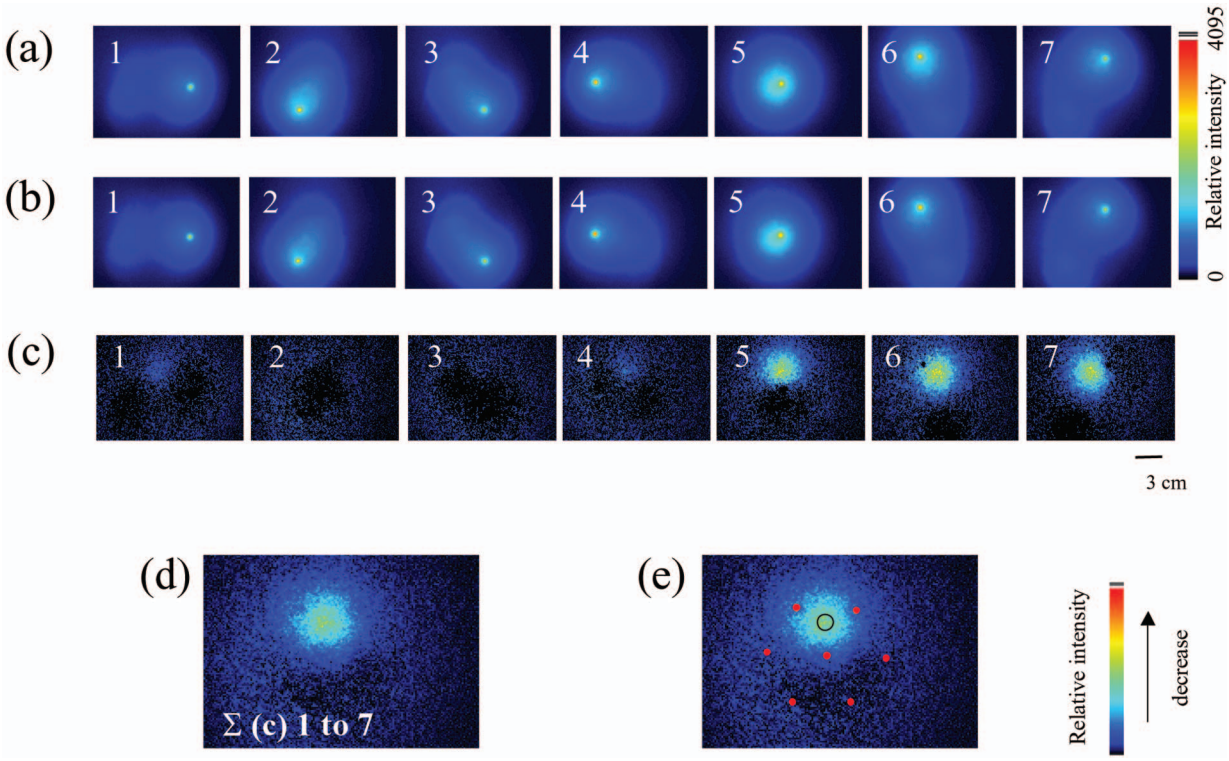

Fig. 4 Detection of black absorber. (a) Images without an absorber; bright spots denote illuminating positions. (b) Images with an absorber. (c) Images subtracted (b) from (a); bright spot predicts the position of absorber. (d) Integrated image of seven images in (c). (e) Illumination spots (red circles) illustrated on the image (d); position of the absorber is shown by a black open circle. Wavelength of 805 nm, which corresponds to an isosbestic point of oxygenated and deoxygenated hemoglobin, was used to capture images.

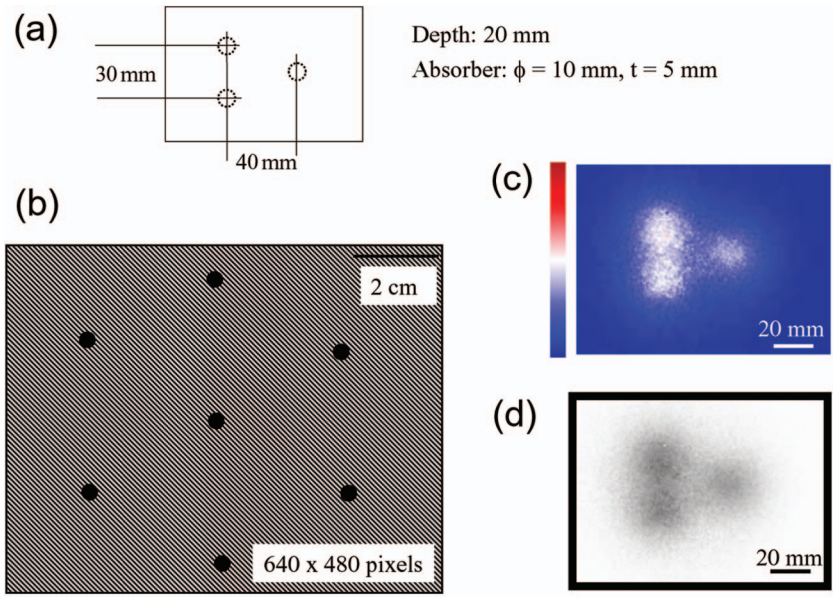

Fig. 5 (a) Position of absorbers buried at the depth of 20 mm in the phantom. (b) Illustration of light illumination position and receiving areas of noncontact B-TRIS. Closed circles indicate the region of illumination and the slash mark indicates the region of detection. (c) Pseudo color image obtained with B-TRIS. (d) Grayscale image of (c). Wavelength of 805 nm was used. Time window of noncontact B-TRIS was 600 ps (between 1800 and 2400 ps).

power for mapping light-absorbing particles buried inside the scattering media in the reflectance mode for the purpose of applying this technology to the human brain mapping.

3.1 *Measurement of Optical Properties of Phantom Sample*

For the phantom, we have used white polyacetal as a light-scattering medium and black polyacetal particles for absorbers. Temporal profiles of light intensity reflected by the large bulk phantom (Fig. 3) were measured by noncontact B-TRIS. Plots of the light intensity (solid lines) and the fitting curve using Patterson's half infinite model[29] are shown in Fig. 3. Their optical properties were obtained by the present system (noncontact B-TRIS) and the conventional fiber-based time-resolved system (TRS-10, Hamamatsu Photonics, Hamamatsu, Japan)[30] and are shown in Table 1. Although there is difference in the wavelength used here, 780 nm for noncontact B-TRIS and 761 and 795 nm for TRS-10, the scattering coefficient ($\mu s'$) obtained by both instruments gave similar results. On the other hand, absorption coefficient (μa) showed about twofold difference between these instruments. This probably indicates that the order $\sim 10^{-3}$ mm^{-1} is the sensitivity limit of μa for B-TRIS and/or TRS-10. However, optical properties of the human brain tissue (cortex) are $\mu s' = \sim 1.00$ mm^{-1} and $\mu a \cong 0.02$ mm^{-1}.[31] The value of μa of the human cortex is about 20 times larger than that of the present phantom sample. Thus, the B-TRIS and TRS-10 may be practical to measure the optical properties of the human brain tissue.

3.2 *Time-Resolved Imaging in Scattering Media*

The captured images and calculation procedures for detecting small absorber particles buried inside the polyacetal phantom are illustrated in Figs. 4(a)–4(d). The illumination spots marked with filled red circles and the position of the absorber marked with an open black circle, where illuminating laser spots were placed hexagonally to cover the imaging area of about 90 mm in diameter, are illustrated in Fig. 4(e) [see also Fig. 2(a)].

Backscattered images from the phantom without an absorber are shown in Fig. 4(a), and the same images with an absorber buried at a depth of 17.5 mm are shown in Fig. 4(b). The absorber is 10 mm in diameter (φ) and 5 mm thick (t). A pulse laser was illuminated sequentially to seven different spots [see light spot in images in Figs. 4(a) and 4(b)], and images were obtained with a 30-ms CCD integration time and a 600-ps time window (1800 to 2400 ps after the laser illumination, see Fig. 8) of the gated intensifier. Images in Fig. 4(c) were obtained by subtracting images of Fig. 4(b) from those of Fig. 4(a), where specularly reflected light, which appeared as bright spots in Figs. 4(a) and 4(b), were removed by subtraction and only diffusely reflected lights were obtained in Fig. 4(c). An integrated image of the seven images in Fig. 4(c) is shown in Fig. 4(d). As referred to in Fig. 4(e), Fig. 4(c) indicates decreases in the reflected signal ("shadow," i.e., light blue and yellow area) just above the absorber (except for numbers 2 and 3, whose illuminating spots are too far from the absorber). The center of the shadow is less than 2 mm from the center of the absorber. Those correspondences occurred not only for the integrated image [Fig. 4(d)] but also for each subtracted image [Fig. 4(c)].

In the present study, the time window was selected to be 600 ps (1800 to 2400 ps after the illumination of the pulse laser), which gave a broadening of the diameter of the shadow [full width at half maximum (FWHM)=25 mm] 2.5 times larger than the actual diameter of the absorber (10 mm). If earlier arriving photons are captured, the backscattered light from the superficial area may become dominant and its intensity may increase. As a result, the signal from deeply buried absorbers (cf. Fig. 8) is lost.

3.3 *Spatial Resolution of B-TRIS*

For noncontact B-TRIS, the sensitivity to the target object depends on the geometry of the illuminator, but the detected position of the target object is probably unaffected by the position or geometry of the detector (Fig. 4), because the detection area of B-TRIS is the whole area (i.e., ~90-mm diameter of field of view using ϕ=150-mm objective lens). The spatial configuration of light illumination and detection of B-TRIS are illustrated in Fig. 5. Figure 5(a) shows the position of three absorbers buried in the phantom. The three absorbers buried at a depth of 20 mm in the phantom. Figure 5(b) shows the region of light illumination (closed circles) and the region of detection (slashed mark region). Images obtained using noncontact B-TRIS, in which individual shadows of three absorbers can be visualized clearly, are shown in Figs. 5(c) and 5(d) [Fig. 5(c), pseudo colored image; Fig. 5(d), black and white image]. Furthermore, the position and shape of shadows obtained by noncontact B-TRIS did not change even when the relative positions of sample and light illumination were changed (data not shown).

Further, to evaluate the spatial resolution of noncontact B-TRIS quantitatively, we placed two absorbers in the phantom at the depth of 20 mm (inset of Fig. 6). The profiles of the reflected light intensity along the line connecting the centers of absorbers are shown in Fig. 6. The time window was set between 1800 and 2400 ps, where the reflected light intensity is at its maximum at a depth of 20 mm (see Fig. 8). One can clearly notice the two separate peaks when the distance of two absorbers is longer than 20 mm. However, two absorbers could be discriminated from a two-dimensional image even when the gap was 15 mm.

3.4 *Sensitivity Depending on the Sample Position*

The uniformity of the sensitivity throughout the target area obtained by noncontact B-TRIS is shown in Fig. 7. We measured peak intensity changes in backscattered light from a single absorber that moved across the field of view, as shown with arrows (trace A and B) in the inset of Fig. 7, where the illumination positions are shown with closed circles. The sensitivity of B-TRIS is relatively flat near the center and it gradually decreases as the target position approaches the edge of the target area. Furthermore, the position of the absorber measured by B-TRIS coincided the actual position with accuracy $<$2 mm as described before.

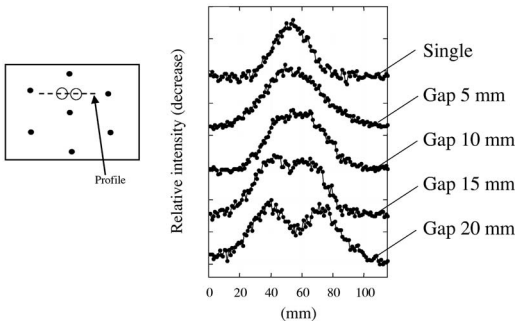

Fig. 6 Profiles of the reflected light intensity along the line connecting centers of the absorbers. Inset is an illustration of two absorbers placed in the phantom at the depth of 20 mm. Wavelength of 805 nm was used, and the time window of noncontact B-TRIS was 600 ps (between 1800 and 2400 ps).

3.5 *Depth Measurement*

Normalized temporal changes in light intensity depending on the depth of the absorbing samples are shown in Fig. 8. As the depth of the absorber increased, the backscattered light path and the time of flight also increased. The peak value of the backscattered light intensity decreases exponentially and the time-of-flight profile is broadened with increasing absorber depth. This result indicates that the present noncontact B-TRIS provides not only the two-dimensional distribution of the absorbers but also their depth information.

4 Discussion

Time-resolved optical imaging methods are powerful for extracting not only temporal but also spatial profiles of target objects. There have been many reports applying time-resolved methods to capture ballistic or banana-shaped propagated light through scattering media by discriminating the specific

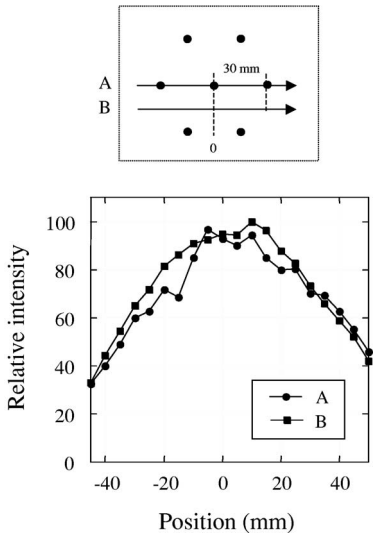

Fig. 7 Top, illustration of illumination (black circles) and detection (white plane) positions of B-TRIS, and traces of absorber (A and B). Bottom, changes in reflected light intensity accompanying the movement of absorber. Experimental conditions were the same as those of Fig. 5.

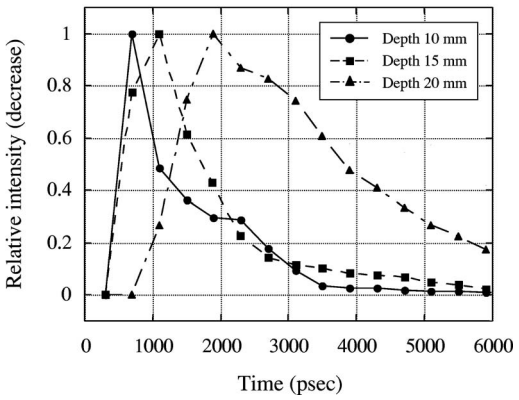

Fig. 8 Changes in normalized light intensity obtained at different depths of the absorber. Configuration of incident optical fibers and an absorber was the same as that shown in Fig. 4(e), but the depth of absorber was changed. Wavelength of 805 nm was used, and each plot was obtained with a time window of 600 ps. The data points indicate the light intensity integrated over the region of 3×3 mm^2 on the phantom surface at a distance of 40 mm from the incident light spot. The absorber was buried in the middle of incident and detection points.

component of scattered light. As described before, advantages of the time-resolved optical measurement system have been demonstrated by many fundamental experiments and human applications: the higher resolving power of optical tomographic schemes using fast-transmitted photons of ultrashort pulses,[27] better depth sensitivity than continuous wave systems,[20,21,32] and the ability to acquire an effective path length using the time-of-flight value.[28] Recently, noncontact imaging systems using near-infrared light and fluorescent probe have been developed to detect cancer tissues.[22,24,26] In the present study, we have developed a noncontact reflective-mode time- resolved imaging system to visualize light absorbing particles placed inside the scattering medium. Our aim is focused on future applications of this system to detect intrinsic signals, such as oxygenated and deoxygenated hemoglobin, for functional mapping in the human head. At present, however, there are several problems to be solved for practical application to functional human brain mapping, such as (1) movement of subject is restricted within a focus area of the detecting objective lens, and (2) the hair is highly critical for injection and detection of light, thus the measurement area is restricted to the hairless region such as the forehead. However, one important merit of this system was that we could actually visualize the shadow of each absorbing particle right above its location, without any interpolation or complicated calculations. Therefore, by extracting a suitable portion of the photons using the time-resolved method, local changes in absorption at a deeper region can be projected perpendicularly onto the surface by taking the shortest path through the scattered medium. This would reduce the annoyance of remapping and interpolation of the data obtained using the source-detector (S-D) imaging system. Although S-D imaging systems are currently used to detect stimulus-induced brain activation in human subjects, the system provides accurate data only when the activation area is larger than the optical pixel size. It is restricted by the S-D distance as well as their positioning.

Another merit of the time-resolved method is the ability to map time-of-flight data of the target sample. Time-of-flight profiles would allow us to know the depth information of the object and allow us to determine absolute concentration changes of absorber such as hemoglobin.

5 Conclusion

We reported the construction of noncontact B-TRIS and its application to *in vitro* experiments. Improvement of spatial resolution and detection of absorbing materials buried in the scattering medium in the reflection mode was shown. Further fundamental experiments using more practical models are required, because the brain has layered structures, which are more complicated than plain phantoms, and blood vessels running near the surface would make interpretation of the data more complicated. We, however, hope that the B-TRIS will become a powerful tool for clinical and cognitive neuroscience research in human subjects.

Acknowledgments

This research was supported by the Breakthrough 21 Project of the Ministry of Posts and Telecommunications of Japan, and in part by Grants-in-Aid from the Nissan Science Foundation of Japan. The authors thank Dr. H. Eda for helpful comments and suggestions.

References

1. M. Moosmann, P. Ritter, I. Krastel, A. Brink, S. Thees, F. Blankenburg, B. Taskin, H. Obrig, and A. Villringer, "Correlates of alpha rhythm in functional magnetic resonance imaging and near infrared spectroscopy," *Neuroimage* **20**, 145–158 (2003).
2. B. M. Mackert, G. Wubbeler, S. Leistner, K. Uludag, H. Obrig, A. Villringer, L. Trahms, and G. Curio, "Neurovascular coupling analyzed non-invasively in the human brain," *NeuroReport* **19**, 63–66 (2004).
3. A. Seiyama, J. Seki, H. C. Tanabe, I. Sase, A. Takatsuki, S. Miyauchi, H. Eda, S. Hayashi, T. Imaruoka, T. Iwakura, and T. Yanagida, "Circulatory basis of fMRI signals: Relationship between changes in the hemodynamic parameters and BOLD signal intensity," *Neuroimage* **21**, 1204–1214 (2004).
4. K. Uludag, J. Steinbrink, M. Kohl-Bareis, R. Wenzel, A. Villringer, and H. Obrig, "Cytochrome-c-oxidase redox changes during visual stimulation measured by near-infrared spectroscopy cannot be explained by a mere cross talk artefact," *Neuroimage* **22**, 109–119 (2004).
5. I. Miyai, H. C. Tanabe, I. Sase, H. Eda, I. Oda, I. Konishi, Y. Tsunazawa, T. Suzuki, T. Yanagida, and K. Kubota, "Cortical mapping of gait in humans: A near-infrared spectroscopic topography study," *Neuroimage* **14**, 1186–1192 (2001).
6. T. Kusaka, K. Kawada, K. Okubo, K. Nagano, M. Namba, H. Okada, T. Imai, K. Isobe, and S. Itoh, "Noninvasive optical imaging in the visual cortex in young infants," *Hum. Brain Mapp* **22**, 122 – 132 (2004).
7. T. Higashi, Y. Sone, K. Ogawa, Y. T. Kitamura, K. Saiki, S. Sagawa, T. Yanagida, and A. Seiyama, "Changes in regional cerebral blood volume in frontal cortex during mental work with and without caffeine intake: Functional monitoring using near-infrared spectroscopy," *J. Biomed. Opt.* **9**, 788–793 (2004).
8. M. N. J. Herrmann, A. C. Ehlis, and A. J. Fallgatter, "Frontal activation during a verbal-fluency task as measured by near-infrared spectroscopy," *Brain Res. Bull.* **30**, 51–56 (2003).
9. T. Suto, M. Fukuda, M. Ito, T. Uehara, and M. Mikuni, "Multichannel near-infrared spectroscopy in depression and schizophrenia: Cognitive brain activation study," *Biol. Psychiatry* **55**, 501–511 (2004).
10. A. Watanabe and T. Kato, "Cerebrovascular response to cognitive tasks in patients with schizophrenia measured by near-infrared spectroscopy," *Schizophr Bull.* **30**, 435–444 (2004).
11. J. Steinbrink, M. Kohl, H. Obrig, G. Curio, F. Syre, F. Thomas, H. Wabnitz, H. Rinneberg, and A. Villringer, "Somatosensory evoked fast optical intensity changes detected noninvasively in the adult human head," *Neurosci. Lett.* **291**, 105–108 (2000).
12. M. Wolf, U. Wolf, J. H. Choi, R. Gupta, L. P. Safonova, L. A. Paunescu, A. Michalos, and E. Gratton, "Functional frequency-domain near-infrared spectroscopy detects fast neuronal signal in the motor cortex," *Neuroimage* **17**, 1868–1875 (2002).
13. M. A. Franceschini and D. A. Boas, "Noninvasive measurement of neuronal activity with near-infrared optical imaging," *Neuroimage* **21**, 372–386 (2004).
14. D. A. Boas, T. Gaudette, G. Strangman, X. Cheng, J. J. A. Marota, and J. B. Mandeville, "The accuracy of near infrared spectroscopy and imaging during focal changes in cerebral hemodynamic," *Neuroimage* **13**, 76–90 (2001).
15. H. Obrig and A. Villringer, "Beyond the visible—Imaging the human brain with light," *J. Cereb. Blood Flow Metab.* **23**, 1–18 (2003).
16. E. Paulesu, R. S. J. Frackowiak, and G. Bottini, "Maps of somatosensory systems," in *Human Brain Function*, R. S. J. Frackowiak, K. J. Friston, C. D. Frith, R. J. Dolan, and J. C. Mazziotta, Eds., pp. 183–242, Academic Press, San Diego (1997).
17. P. Petrovic, K. M. Petersson, P. Hansson, and M. Ingvar, "A regression analysis study of the primary somatosensory cortex during pain," *Neuroimage* **16**, 1142–1150 (2002).
18. J. T. E. Richardson, *Imagery*, Psychology Press, London (1999).
19. A. D. Boas, A. M. Dale, and M. A. Franceschini, "Diffuse optical imaging of brain activation: Approaches to optimizing image sensitivity, resolution, and accuracy," *Neuroimage* **23**, 5275–5288 (2004).
20. J. Selb, J. J. Stott, M. A. Franceschini, A. G. Sorenson, and D. A. Boas, "Improved sensitivity to cerebral dynamics during brain activation with a time-gated optical system: Analytical model and experimental validation," *J. Biomed. Opt.* **10**(1), 011013 (2005).
21. B. Montcel, R. Chabrier, and P. Poulet, "Detection of cortical activation with timeresolved diffuse optical methods," *Appl. Opt.* **44**, 1942–1947 (2005).
22. A. B. Thompson, D. J. Hawrysz, and E. M. Sevick-Muraca, "Near-infrared contrast-enhanced imaging with area illumination and area detection: The forward imaging problem," *Appl. Opt.* **42**, 4125–4136 (2003).
23. R. B. Schulz, J. Ripoll, and V. Ntziachristos, "Noncontact optical tomography of turbid media," *Opt. Lett.* **28**, 1701–1703 (2003).
24. R. B. Schulz, J. Ripoll, and V. Ntziachristos, "Experimental fluorescence tomography of tissues with noncontact measurements," *IEEE Trans. Med. Imaging* **23**, 492–500 (2004).
25. G. M. Turner, G. Zacharakis, A. Soubret, J. Ripoll, and V. Ntziachristos, "Complete-angle projection diffuse optical tomography by use of early photons," *Opt. Lett.* **30**, 409–411 (2005).
26. R. Roy, A. B. Thompson, A. Godavarty, and E. M. Sevick-Muraca, "Tomographic fluorescence imaging in tissue phantoms: A novel reconstruction algorithm and imaging geometry," *IEEE Trans. Med. Imaging* **24**, 137–154 (2005).
27. H. Eda, I. Oda, Y. Ito, Y. Wada, Y. Oikawa, Y. Tsunazawa, M. Takada, Y. Tsuchiya, Y. Yamashita, M. Oda, A. Sassaroli, Y. Yamada, and M. Tamura, "Multi-channel time-resolved optical tomographic imaging system," *Rev. Sci. Instrum.* **70**, 3595–3602 (1999).
28. D. T. Delpy, M. Cope, P. van der Zee, S. Arridge, S. Wray, and J. Wyatt, "Estimation of optical pathlength through tissue from direct time flight measurement," *Phys. Med. Biol.* **33**, 1433–1442 (1988).
29. M. S. Patterson, B. Chance, and B. C. Wilson, "Time resolved reflectance and transmittance for the non-invasive measurement of tissue optical properties," *Appl. Opt.* **28**, 2331–2336 (1989).
30. M. Oda, Y. Yamashita, T. Nakano, A. Suzuki, K. Shimizu, I. Hirano, F. Shimomura, E. Ohmae, T. Suzuki, and Y. Tsuchiya, "Nearinfrared time-resolved spectroscopy system for tissue oxygenation monitor," *Proc. SPIE* **3597**, 611–616 (1999).
31. F. Bevilacqua, D. Piguet, P. Marquet, J. D. Gross, B. J. Tromberg, and C. Depeursinge, "*In vivo* local determination of tissue optical properties: Applications to human brain," *Appl. Opt.* **38**, 4939–4950 (1999).
32. A. Liebert, H. Wabnitz, J. Steinbrink, H. Obrig, M. Moller, R. Macdonald, A. Villringer, and H. Rinneberg, "Time-resolved multidistance near-infrared spectroscopy of the adult head: Intracerebral and extracerebral absorption changes from moments of distribution of time of flight of photons," *Appl. Opt.* **43**, 3037–3047 (2004).